
INTERVENTIONALLY CONSISTENT SURROGATES FOR AGENT-BASED SIMULATORS

PREPRINT

Joel Dyer
University of Oxford

Nicholas Bishop
University of Oxford

Yorgos Felekis
University of Warwick

Fabio Massimo Zennaro
University of Bergen

Anisoara Calinescu
University of Oxford

Theodoros Damoulas
University of Warwick

Michael Wooldridge
University of Oxford

December 19, 2023

ABSTRACT

Agent-based simulators provide granular representations of complex intelligent systems by directly modelling the interactions of the system’s constituent agents. Their high-fidelity nature enables hyper-local policy evaluation and testing of *what-if* scenarios, but is associated with large computational costs that inhibits their widespread use. Surrogate models can address these computational limitations, but they must behave consistently with the agent-based model under policy interventions of interest. In this paper, we capitalise on recent developments on causal abstractions to develop a framework for learning interventionally consistent surrogate models for agent-based simulators. Our proposed approach facilitates rapid experimentation with policy interventions in complex systems, while inducing surrogates to behave consistently with high probability with respect to the agent-based simulator across interventions of interest. We demonstrate with empirical studies that observationally trained surrogates can misjudge the effect of interventions and misguide policymakers towards suboptimal policies, while surrogates trained for interventional consistency with our proposed method closely mimic the behaviour of an agent-based model under interventions of interest.

Keywords Agent-based models · causal abstraction · policy interventions · surrogate models

1 Introduction

Agent-based models (ABMs) are a powerful tool for modelling complex decision-making systems across application domains, including the social sciences (Baptista et al., 2016), epidemiology (Kerr et al., 2021), and finance (Cont, 2007). Such models provide high-fidelity and granular representations of intricate systems of autonomous, interacting, and decision-making agents by modelling the system under consideration at the level of its individual constituent actors. In this way, ABMs enable decision-makers to experiment with, and understand the potential consequences of, policy interventions of interest, thereby allowing for more effective control of the potentially deleterious effects that arise from the endogenous dynamics of the real-world system. In economic systems, for example, such policy interventions may take the form of imposed limits on loan-to-value ratios in housing markets as a means for attenuating housing price cycles (Baptista et al., 2016), while in epidemiology, such interventions may take the form of (non-)pharmaceutical interventions to inhibit the transmission of a disease (Kerr et al., 2021).

Whilst ABMs promise many benefits, their complexity generally necessitates the use of simulation studies to understand their behaviours, and their granularity can result in large computational costs even for single forward simulations. In many cases, such costs can be prohibitively large, presenting a barrier to their use as synthetic test environments for potential policy interventions in practice. Moreover, the high-fidelity data generated by ABMs can be difficult for policymakers to interpret and relate to policy interventions that act system-wide (Haldane and Turrell, 2018). This motivates the development of simpler *surrogate* models which model the underlying system at a higher level of abstraction. Such surrogates can be used in place of ABMs for downstream tasks where computational resources are

limited. In addition, surrogates may be viewed as interpretable explanations for ABM behaviour, and they allow for rapid testing of population-wide interventions which may be difficult to implement or test within an ABM.

However, for surrogates to be useful in downstream tasks involving experimentation with possible policy interventions, they must preserve ABM dynamics under the external policy interventions of interest. Without imposing this condition on the constructed surrogate, there is no guarantee that the surrogate will behave similarly under external policy interventions, which in turn may lead policy-makers away from effective policies and towards suboptimal interventions. Existing methods in the literature typically apply off-the-shelf machine learning methods to learn surrogates in an observational manner, failing to account for interventional consistency.

To address this issue, we build on recent developments in *causal abstraction learning* (Beckers and Halpern, 2019; Zennaro et al., 2023a). We view the ABM and surrogate model as *structural causal models* (Pearl, 2009), and propose a framework for constructing and learning surrogate models for complex and expensive agent-based simulators that are *interventionally consistent*, in the sense that they (approximately) preserve the behaviour of the ABM under equivalent policy interventions. This perspective enables treating the surrogate model as a causal abstraction of the ABM and reveals the importance of including interventional data from the ABM in the learning of surrogate models, given that interventions induce different distributions as, explained by the formalism of structural causal models. We motivate our proposed methodology theoretically, and demonstrate with simulation studies that our approach permits us to learn an abstracted surrogate model for an epidemiological ABM that behaves consistently in multiple interventional regimes.

Our approach establishes for the first time a connection between ABMs and causal abstraction, allowing researchers in the field of ABMs to draw on the rich literature in causality for integrating causal knowledge, evaluating *what-if* scenarios, and learning new abstracted models with guarantees about interventional consistency. This, in turn, will enable decision- and policy-makers to experiment with policy interventions in cheaper and more interpretable surrogate models, with assurance that the error introduced by experimenting at a higher level of abstraction is low.

2 Background

We first review elements of causal inference, following the framework of Pearl (2009), and elucidate on the connection between structural causal models and ABMs. We also review the notion of exact transformation between structural causal models, which serves as the theoretical motivation for our framework.

2.1 Structural Causal Models

A structural causal model (SCM), is a rigorous model describing a causal system. Each component of the system is represented by a variable, whose behaviour and relation to other components is expressed by a structural equation.

Definition 1 (SCMs (Pearl, 2009)). *A structural causal model \mathcal{M} consists of a tuple $\langle \mathbf{X}, \mathbf{U}, \mathcal{F}, \mathbb{P}(\mathbf{U}) \rangle$ where:*

- $\mathbf{X} = \{X_i\}_{i=1}^n$, is a finite set of endogenous random variables X_i each with domain $\text{dom}[X_i]$;
- $\mathbf{U} = \{U_i\}_{i=1}^n$, is a finite set of exogenous random variables, each with domain $\text{dom}[U_i]$ and each associated with an endogenous variable;
- $\mathcal{F} = \{f_i\}_{i=1}^n$, is a finite set of measurable structural functions, one for each endogenous variable defined as $f_i : \text{dom}[PA(X_i)] \times \text{dom}[U_i] \rightarrow \text{dom}[X_i]$, where $PA(X_i) \subseteq \mathbf{X} \setminus X_i$.
- $\mathbb{P}_{\mathcal{M}}(\mathbf{U})$ is a joint probability distribution over the exogenous variable factorizing as $\prod_{i=1}^n \mathbb{P}_{\mathcal{M}}(U_i)$.

The model \mathcal{M} is associated with a Directed Acyclic Graph (DAG) $\mathcal{G}_{\mathcal{M}} = \langle \mathcal{V}, \mathcal{E} \rangle$ where the set \mathcal{V} of vertices is given by $\mathbf{X} \cup \mathbf{U}$ and the set \mathcal{E} of edges is given by $\{(S_j, X_i) | S_j \in PA(X_i) \cup \{U_i\}\}_{i=1}^n$.

Definition 1 conforms to the standard definition of a *Markovian SCM* (see Appendix A for an explanation of the underlying assumptions). Thanks to the measurability of the structural functions in \mathcal{F} , the probability distribution $\mathbb{P}_{\mathcal{M}}(\mathbf{U})$ over the exogenous variables can be pushed forward over the endogenous variables, defining the probability distribution $\mathbb{P}_{\mathcal{M}}(\mathbf{X}) = \mathcal{F}_{\#}(\mathbb{P}_{\mathcal{M}}(\mathbf{U}))$. Joint probability distributions $\mathbb{P}_{\mathcal{M}}(\mathbf{S})$ can then be defined for any subset $\mathbf{S} \subseteq \mathbf{X}$.

External interventions on the system by an experimenter can be represented in an SCM through changes in the structural functions. In this work, we focus our attention on hard interventions, which assign fixed values to a subset of endogenous variables.

Definition 2 (Interventions (Pearl, 2009)). *Given an SCM \mathcal{M} , $\mathbf{S} \subseteq \mathbf{X}$ and a set of values \mathbf{s} realizing \mathbf{S} , an intervention $\iota = \text{do}(\mathbf{S} = \mathbf{s})$, is an operator that replaces each function f_i associated with S_i with constant s_i .*

The intervention $\iota = \text{do}(\mathbf{S} = \mathbf{s})$ induces a new *post-intervention* SCM, $\mathcal{M}_\iota = \langle \mathbf{X}, \mathbf{U}, \mathcal{F}_\iota, \mathbb{P}(\mathbf{U}) \rangle$, identical to the original one, except for the set of structural functions \mathcal{F}_ι where the functions f_i are replaced with the constants s_i . The probability distribution of \mathcal{M}_ι is computed as $\mathbb{P}_{\mathcal{M}_\iota}(\mathbf{X} \setminus \mathbf{S})$. Graphically, the intervention ι mutilates the DAG of \mathcal{M} by removing the incoming edges in each variable S_i .

We use \mathcal{I} to denote a set of feasible interventions on the SCM \mathcal{M} that are relevant to a policymaker. Intervention sets are equipped with a natural partial ordering: let $\iota_1 = (\mathbf{S} = \mathbf{s})$ and $\iota_2 = (\mathbf{T} = \mathbf{t})$; then $\iota_1 \preceq \iota_2$ iff (i) $\mathbf{S} \subseteq \mathbf{T}$, and (ii) for each $S_i = T_i$ it holds $s_i = t_i$; informally, ι_1 intervenes on a subset of the variables that ι_2 intervenes on, and it sets the same values as ι_2 .

2.2 Agent-based Models as SCMs

Observe that an ABM can be modelled as a SCM by expressing its implicit underlying causal structure. Practically, this entails encoding quantities of interest as endogenous variables, deterministic dynamics into structural equations, and factoring sources of randomness into exogenous variables. Example 1 shows how a common ABM of epidemics can be described as a SCM.

Example 1 (Spatial SIRS ABM). *We consider a susceptible-infected-recovered-susceptible (SIRS) epidemic model on an $L \times L$ lattice of cells, each of which represents one of $N = L^2$ agents. The state of each agent can be 0, 1, or 2, respectively indicating that the agent is disease-free and susceptible to infection, infected, or is recovered from a recent infection. The infection status of all agents at discrete time step $t \in \llbracket 0, T \rrbracket$ is written as $\mathbf{x}_t \in \{0, 1, 2\}^N$, where T is the total number of simulated time steps, and $\llbracket l, m \rrbracket = \{l, l+1, \dots, m-1, m\}$ for integers $l \leq m$. The states $\mathbf{x}_{t,n}$ of each of the agents $n \in \llbracket 1, N \rrbracket$ are updated synchronously as follows for $t \in \llbracket 0, T-1 \rrbracket$:*

- If $\mathbf{x}_{t,n} = 0$, then $\mathbf{x}_{t+1,n} = 1$ with probability

$$p_{t,n}(\alpha_{t+1}) = 1 - (1 - \alpha_{t+1})^{\sum_{n' \in \mathcal{N}_n} \mathbb{I}[\mathbf{x}_{t,n'}=1]} \quad (1)$$

where \mathcal{N}_n is the von Neumann neighbourhood for cell n ; else remain susceptible.

- If $\mathbf{x}_{t,n} = 1$, then $\mathbf{x}_{t+1,n} = 2$ with probability β_{t+1} ; else remain infected.
- If $\mathbf{x}_{t,n} = 2$, then $\mathbf{x}_{t+1,n} = 0$ with probability γ_{t+1} ; else remain recovered.

In the above, $\boldsymbol{\theta}_t = (\alpha_t, \beta_t, \gamma_t) \in [0, 1]^3$ are the model parameters determining the transition probabilities between states. While these may vary over time, the simplest case consists of assigning all $\boldsymbol{\theta}_t$ the same vector,

$$\boldsymbol{\theta}_t = \mathbf{v} \quad \forall t \in \llbracket 1, T \rrbracket. \quad (2)$$

The model is initialised by infecting each agent in the model at initial time $t = 0$ with probability $I_0 \in [0, 1]$. The value of I_0 for any forward simulation of the model can be chosen by drawing a random variable a from some distribution on $[0, 1]$ and setting

$$I_0 = a. \quad (3)$$

With this model in place, lockdowns over some time period $t_l : t_l + \Delta$ of length $\Delta \geq 0$ can be modelled (crudely) by setting $\boldsymbol{\theta}_{t_l:t_l+\Delta} = (0, \beta, \gamma)$ for $\beta, \gamma \in [0, 1]$.

To express this ABM as an SCM, we define the following:

Endogenous variables These consist of the variables of interest that may be set by the policymaker: I_0 , $\{\mathbf{x}_t\}_{0 \leq t \leq T}$, and $\{\boldsymbol{\theta}_t\}_{1 \leq t \leq T}$.

Exogenous variables The model as described above is initialised randomly according to a , \mathbf{v} , and a collection $\mathbf{u}_0 = (\mathbf{u}_{0,n})_{1 \leq n \leq N}$ of N random variables distributed as $\mathcal{U}(0, 1)$, the n th of which decides whether agent n is infected at time $t = 0$. Similarly, further collections \mathbf{u}_t , $t \in \llbracket 1, T \rrbracket$ of $\mathcal{U}(0, 1)$ random variables decide how each agent updates their state at each time step. Thus the exogenous variables for the model are a , \mathbf{v} , and the \mathbf{u}_t for $t \in \llbracket 0, T \rrbracket$.

2.3 Causal Abstractions

Beside expressing interventions more rigorously, viewing an ABMs as a SCMs allows one to take advantage of the theory of causal abstraction to formalise the relationship between an ABM and a surrogate model. Indeed, causal abstraction provides a framework for relating SCMs representing an identical system at different levels of granularity. The notion of exact transformation formalizes this relation, providing a framework to relate complex models, such as ABMs, to simpler top-down models while preserving causal structure.

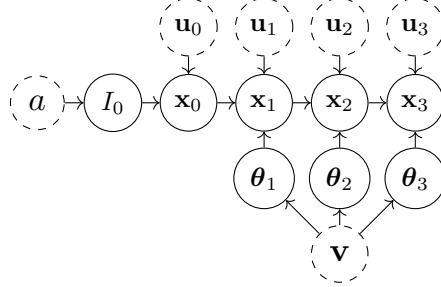


Figure 1: The directed acyclic diagram induced by the structural causal model corresponding to the spatial SIRS agent-based simulator for $T = 3$ time steps.

Definition 3 (τ - ω Exact Transformation (Rubenstein et al., 2017)). *Given two SCMs, \mathcal{M} and \mathcal{M}' , with respective intervention sets \mathcal{I} and \mathcal{I}' , a τ - ω transformation is a pair (τ, ω) consisting of a map $\tau : \text{dom}[\mathbf{X}] \rightarrow \text{dom}[\mathbf{X}']$ and a surjective, order-preserving map $\omega : \mathcal{I} \rightarrow \mathcal{I}'$. An exact τ - ω transformation is a τ - ω transformation such that*

$$\tau_{\#}(\mathbb{P}_{\mathcal{M}_{\iota}}) = \mathbb{P}_{\mathcal{M}'_{\omega(\iota)}}, \forall \iota \in \mathcal{I}. \quad (4)$$

Structural equations Equations 2 and 3, respectively, define the structural equations f_{θ_t} and f_{I_0} for the endogenous variables θ_t and I_0 . The structural equation $f_{\mathbf{x}_{0,n}}$ for each $\mathbf{x}_{0,n}$, $n \in \llbracket 1, N \rrbracket$ can furthermore be written as

$$\mathbf{x}_{0,n} = f_{\mathbf{x}_{0,n}}(u_{0,n}, I_0) = \mathbb{I}[u_{0,n} < I_0]. \quad (5)$$

Finally, the three update rules for \mathbf{x}_t described above can be written concisely with the following structural equations for $t \in \llbracket 0, T-1 \rrbracket$:

$$\begin{aligned} \mathbf{x}_{t+1,n} &= f_{\mathbf{x}_{t+1,n}}(\theta_{t+1}, u_{t+1,n}, \mathbf{x}_{t,n}) \\ &= \mathbb{I}[\mathbf{x}_{t,n} = 0] \cdot \mathbb{I}[u_{t+1,n} < p_{t,n}(\alpha_{t+1})] + \mathbb{I}[\mathbf{x}_{t,n} = 1] \cdot (1 + \mathbb{I}[u_{t+1,n} < \beta_{t+1}]) \\ &\quad + 2\mathbb{I}[\mathbf{x}_{t,n} = 2] \cdot (1 - \mathbb{I}[u_{t+1,n} < \gamma_{t+1}]), \end{aligned} \quad (6)$$

Distribution over the exogenous variables The stochastic behaviour over the exogenous variables is fully specified by the distribution over a and \mathbf{v} , together with a $\mathcal{U}(0, 1)$ distribution over each \mathbf{u}_t .

The underlying graph The DAG corresponding to this SCM is shown in Figure 1 for $T = 3$.

In this model, interventions in the form of, for example, a lockdown can be (crudely) modelled by intervening on one or more of the θ_t as $\text{do}(\theta_t = (0, \beta, \gamma))$ for some $\beta, \gamma \in [0, 1]$, while in the observational regime the θ_t will all be assigned the same value.

An exact τ - ω transformation constitutes a form of abstraction between probabilistic causal models (Beckers et al., 2020) with the guarantee of commutativity between intervention and transformation as detailed in Figure 2: intervening via ι and then abstracting produces the same result as abstracting first and then intervening via $\omega(\iota)$. The map τ describes corresponding states in each of the models, while the map ω describes corresponding interventions in each model. In the following, whenever the map τ is clear from context, we shorthand the pushforward measure $\tau_{\#}(\mathbb{P}_{\mathcal{M}_{\iota}})$ as $\mathbb{P}_{\mathcal{M}'_{\omega(\iota)}}$.

An exact τ - ω transformation between the SCM \mathcal{M} underlying an ABM and the SCM \mathcal{M}' underlying the candidate surrogate model would (a) certify that the surrogate preserves the causal structure of interest, (b) allow to interpret the emergent causal structure of the ABM through \mathcal{M}' , and (c) provide guarantees of interventional consistency when a policymaker would study real-world interventions through the surrogate model.

3 Abstraction Error

Unfortunately, it is unrealistic to assume that an exact τ - ω transformation exists between an ABM and a surrogate. In fact, ABMs are often developed for problem settings where simple top-down models fail to fully capture the dynamics of interest. In such cases, a more pragmatic goal is to find an approximate abstraction (Beckers et al., 2020) from the ABM to the surrogate. For this reason we define the *abstraction error*.

Definition 4 (Abstraction error). *Let (τ, ω) be a τ - ω transformation between two SCMs \mathcal{M} and \mathcal{M}' with respective intervention sets \mathcal{I} and \mathcal{I}' . Given a statistical divergence d between distributions, and a distribution η over the intervention set \mathcal{I} , we define the abstraction error as follows:*

$$d_{\tau, \omega}(\mathcal{M}, \mathcal{M}') = \mathbb{E}_{\iota \sim \eta} \left[d \left(\tau_{\#}(\mathbb{P}_{\mathcal{M}_{\iota}}), \mathbb{P}_{\mathcal{M}'_{\omega(\iota)}} \right) \right]. \quad (7)$$

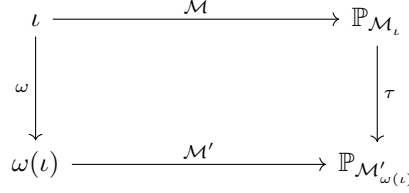


Figure 2: Computing $\tau_{\#}(\mathbb{P}_{\mathcal{M}_l})$, corresponds to moving right then down in the diagram. That is, running the intervention l in a base model \mathcal{M} such as an ABM. Likewise, computing $\mathbb{P}_{\mathcal{M}'_{\omega(l)}}$ corresponds to moving down then right. That is, running the intervention $\omega(l)$ in an abstracted model \mathcal{M}' such as a surrogate. If (τ, ω) is an exact transformation, then the diagram is commutative for all interventions. That is, $\tau_{\#}(\mathbb{P}_{\mathcal{M}_l}) = \mathbb{P}_{\mathcal{M}'_{\omega(l)}}$ for all $l \in \mathcal{I}$.

A τ - ω transformation is α -approximate for some $\alpha \in \mathbb{R}_{\geq 0}$ if $d_{\tau, \omega}(\mathcal{M}, \mathcal{M}') \leq \alpha$.

The distributional distance d describes the similarity between distributions over states of the surrogate model. A τ - ω abstraction with low abstraction error implies that $\tau_{\#}(\mathbb{P}_{\mathcal{M}_l})$ is close to $\mathbb{P}_{\mathcal{M}'_{\omega(l)}}$ in expectation with respect to the interventional distribution η . If the $d(\tau_{\#}(\mathbb{P}_{\mathcal{M}_l}), \mathbb{P}_{\mathcal{M}'_{\omega(l)}}$) is zero for all interventions $l \in \mathcal{I}$, then (τ, ω) is an exact transformation. Abstraction error is summarised pictorially in Figure 3.

Definition 4 differs from previously defined notions of abstraction error in the causal abstraction literature. Whilst Beckers et al. (2020) employ a maximum over interventions, we instead take an expectation over a fixed interventional distribution η . This is motivated by the fact that policymakers will often hold prior preferences over possible interventions, which may, for example, reflect the cost of implementing each intervention in the real world. Through the specification of η , one may implicitly favour surrogates which perform well with respect to interventions of high interest. Further discussion is provided in Appendix B.

4 Method

The definitions of abstraction and abstraction error provide us with a grounded framework for learning surrogates, and, in the remainder, we assume that the base model \mathcal{M} is always implicitly represented by an ABM. Our goal is to identify a surrogate model which is interventionally consistent with a given ABM. Specifically, given a set of candidate surrogate models \mathfrak{M} , we aim to identify a surrogate model and a τ - ω transformation that minimises the abstraction error.

To proceed, we assume that \mathfrak{M} is induced by a parameterised family $\{\mathcal{M}^{\psi} : \psi \in \Psi\}$ of differentiable surrogate simulators with tractable probability mass or density function q^{ψ} . Here, \mathcal{M}^{ψ} denotes the causal model induced by a surrogate with parameters ψ , and Ψ denotes the set of feasible parameter values. When clear from context, we refer to each surrogate by their corresponding parameter value $\psi \in \Psi$. Such a family of surrogate models can be constructed through a composition of differential equation- or deep learning-based modelling, in combination with probability distributions with reparameterisable sampling procedures; an example of such a composition, of which we make use in the experiments presented in Section 5, is a latent neural ordinary differential equation model (Rubanova et al., 2019). We further assume only the ability to sample from $\tau_{\#}(\mathbb{P}_{\mathcal{M}})$, which amounts to running the ABM and applying τ to the output.

Generally speaking, policymakers know what macroscopic quantities are of interest when modelling a complex system, and how to aggregate the microscopic variables into global statistics. For example, in macroeconomic settings, policymakers will often be concerned with aggregate quantities such as unemployment rates or aggregate demand, which can be derived from the state of the agents. We thus assume access to a pre-specified map τ defining the aggregate, emergent quantities of interest to the policymaker.

Hence, to find an appropriate τ - ω transformation, we need only identify an intervention map ω^* between \mathcal{I} and \mathcal{I}' . To limit computational burden, we select ω^* from a parameterised family $\Omega := \{\omega^{\phi} : \phi \in \Phi\}$ with parameters ϕ ranging over the set Φ . For example, ϕ may correspond to the weights of a neural network. As with surrogates, we refer to each feasible intervention map via their corresponding parameter value $\phi \in \Phi$.

We then select ϕ^* and ψ^* jointly by minimising $d_{\tau, \omega}(\mathcal{M}, \mathcal{M}^{\psi})$ over $\Omega \times \mathfrak{M}$:

$$\phi^*, \psi^* = \arg \min_{\phi \in \Phi, \psi \in \Psi} d_{\tau, \omega^{\phi}}(\mathcal{M}, \mathcal{M}^{\psi}).$$

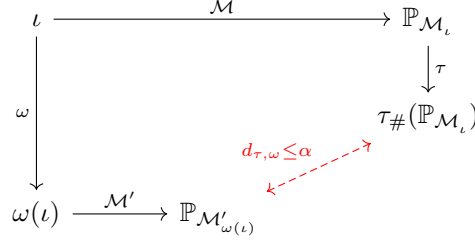


Figure 3: When computing abstraction error, we compare the distributions $\tau_{\#}(\mathbb{P}_{\mathcal{M}_\iota})$ and $\mathbb{P}_{\mathcal{M}'_{\omega(\iota)}}$ for each intervention ι using the divergence $d_{\tau,\omega}$, as indicated by the red dotted arrow. If the divergence is zero then we recover the commutative diagram in Figure 2.

Since each element of \mathfrak{M} has a differentiable and tractable distribution, a convenient choice of discrepancy d is the Kullback-Leibler (KL) divergence:

$$d\left(\tau_{\#}(\mathbb{P}_{\mathcal{M}_\iota}), \mathbb{P}_{\mathcal{M}'_{\omega(\iota)}}\right) = \mathbb{E}_{\mathbb{P}_{\mathcal{M}_\iota}} \left[\log \frac{d\mathbb{P}_{\mathcal{M}_\iota}^{\#}}{d\mathbb{P}_{\mathcal{M}'_{\omega(\iota)}}} \right]. \quad (8)$$

The KL divergence can be minimised with gradient assisted optimisation procedures, in which a Monte Carlo estimate of the gradient is obtained as

$$\nabla_{\phi,\psi} d_{\tau,\omega}(\mathcal{M}, \mathcal{M}^\psi) \approx \frac{1}{B} \sum_{b=1}^B -\nabla_{\phi,\psi} \log q_{\omega(\iota^{(b)})}^\psi(\mathbf{y}^{(b)})$$

where $\iota^{(b)} \sim \eta$, $\mathbf{y}^{(b)} \sim \tau_{\#}(\mathbb{P}_{\mathcal{M}_{\iota^{(b)}}})$, $q_{\omega(\iota)}^\psi$ is the probability mass or density function associated with $\mathcal{M}_{\omega(\iota)}^\psi$, and $B \geq 1$ is the size of a batch drawn from $R \geq B$ training examples from the joint distribution over the $\iota^{(b)}$ and $\mathbf{y}^{(b)}$. After the pair (ϕ^*, ψ^*) have been selected, we may generate data from the macro model for ABM intervention ι by sampling from $\mathbb{P}_{\mathcal{M}'_{\omega(\iota)}}$.

In practice, the experimenter may be interested in only a subset of the endogenous variables of the two SCMs. In this case, the abstraction error we consider can instead be defined with respect to this subset, and the likelihood evaluations required in the optimisation procedure described above can be understood to contain an implicit marginalisation over the auxiliary variables that are excluded from consideration.

4.1 Theory

Definition 4 is closely related to exact transformations:

Proposition 1. *Fix an interventional distribution η and let d be any statistical divergence. Additionally, let (τ, ω) be a τ - ω transformation between two SCMs \mathcal{M} and \mathcal{M}' . If τ - ω is 0-approximate ($d_{\tau,\omega}(\mathcal{M}, \mathcal{M}') = 0$), then we have η -almost-surely*

$$\tau_{\#}(\mathbb{P}_{\mathcal{M}_\iota}) = \mathbb{P}_{\mathcal{M}'_{\omega(\iota)}}.$$

In particular, when \mathcal{I} is finite and $\eta(\iota) > 0 \forall \iota \in \mathcal{I}$, then any 0-approximate τ - ω transformation is an exact τ - ω transformation between the models \mathcal{M} and \mathcal{M}' . Note that any f -divergence with strictly convex f , such as the KL divergence, is a statistical divergence.

Definition 4 employs an expectation over an interventional distribution. As a result, even when the abstraction error is low, there may still be a large discrepancy between $\tau_{\#}(\mathbb{P}_{\mathcal{M}_\iota})$ and $\mathbb{P}_{\mathcal{M}'_{\omega(\iota)}}$ for some fixed intervention $\iota \in \mathcal{I}$. Put differently, running the surrogate with intervention $\omega(\iota)$ may be a poor proxy for running the ABM with intervention ι .

The following proposition provides an upper bound on the divergence associated with any intervention sampled from the interventional distribution η when d is the KL-divergence and the ABM state space is finite.

Proposition 2. *Let d be the KL divergence. Moreover, let $\mathcal{C}E_\iota$ denote the cross-entropy of $\mathbb{P}_{\mathcal{M}'_{\omega(\iota)}}$ with respect to $\tau_{\#}(\mathbb{P}_{\mathcal{M}_\iota})$:*

$$\mathcal{C}E_\iota := \mathbb{E}_{\mathbf{Y} \sim \tau_{\#}(\mathbb{P}_{\mathcal{M}_\iota})} \left[-\log q_{\omega(\iota)}(\mathbf{Y}) \right].$$

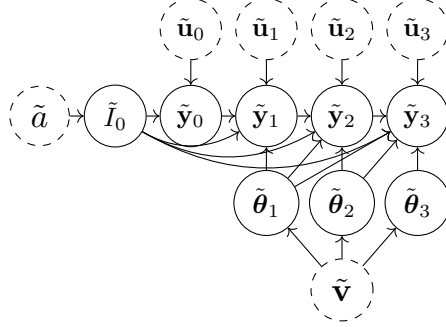


Figure 4: The directed acyclic graph diagram induced by the SCMs corresponding to the surrogate families for $T = 3$.

Assume $\text{dom}[\mathbf{X}]$ is finite. Then for all $\varepsilon > 0$,

$$\mathbb{P}_\eta \left(d \left(\tau_{\#}(\mathbb{P}_{\mathcal{M}_t}), \mathbb{P}_{\mathcal{M}'_{\omega(t)}} \right) \geq \varepsilon \right) \leq \frac{\mathbb{E}_{\iota \sim \eta}[\mathcal{CE}_t]}{\varepsilon}.$$

Evaluating the density associated with $\tau_{\#}(\mathbb{P}_{\mathcal{M}_t})$ and, by extension, the abstraction error is often not possible for ABMs due to their complexity. In contrast, the upper bound in Proposition 2 relies only on the cross-entropy which can be estimated with finite samples.

5 Case Study

In this section, we consider a case study in which we learn interventionally consistent surrogate macromodels for the spatial SIRS ABM described in Example 1. We consider three families of surrogate macromodels with endogenous variables $\tilde{I}_0 \in [0, 1]$, $\tilde{\theta}_t \in \mathbb{R}_{\geq 0}^3$ for $t \in \llbracket 1, T \rrbracket$, and $\tilde{y}_t \in \{(a, b, c) \mid a, b, c \in \llbracket 0, N \rrbracket, a + b + c = N\}$ for $t \in \llbracket 0, T \rrbracket$. The DAGs underlying the SCMs of each of these three families can be drawn as in Figure 4, and the three families differ only in the form of the structural equations mapping from \tilde{I}_0 and $\tilde{\theta}_{0:t}$ to the \tilde{y}_t . Throughout, we let q^ψ be a Multinomial emission distribution and ψ be trainable parameters of these structural equations.

Surrogate family 1 consists of a latent ODE (LODE) constructed by placing q^ψ onto the classical SIRS ODE, such that the ODE's three state variables (which take values in the two-simplex) index the class probabilities of q^ψ . Here, $\psi = \emptyset$.

Surrogate family 2 consists of a latent ODE-RNN (LODE-RNN) constructed by running a recurrent neural network (RNN) with trainable parameters ψ over the output of the classical SIRS ODE. The RNN output then indexes the class logits of q^ψ .

Surrogate family 3 consists of a latent RNN (LRNN) constructed by running an RNN with trainable parameters ψ over the $\tilde{\theta}_t$, where the output of the RNN at each $t \in \llbracket 0, T \rrbracket$ indexes the class logits of q^ψ .

Given $\tilde{\theta}_{1:T}, \tilde{I}_0$, these surrogate macromodels enjoy tractable likelihood functions given by

$$q^\psi(\tilde{y}_{0:T} \mid \tilde{\theta}_{1:T}, \tilde{I}_0) = q^\psi(\tilde{y}_0 \mid \tilde{I}_0) \prod_{t=1}^T q^\psi(\tilde{y}_t \mid \tilde{\theta}_{1:t}, \tilde{I}_0).$$

We provide further details in Appendix E.

5.1 Interventions and the τ - ω Transformation

We consider two subsets of interventions at the level of the ABM. Denoting

$$\begin{aligned} \iota_{\mathbf{v}, a} &= \text{do}(\boldsymbol{\theta}_{1:T} = \mathbf{v}, I_0 = a), \\ \iota_{\mathbf{v}, a, t_l} &= \text{do}(\boldsymbol{\theta}_{1:t_l-1} = \mathbf{v}, \boldsymbol{\theta}_{t_l:t_l+5} = \mathbf{v} \odot (0, 1, 1), \\ &\quad \boldsymbol{\theta}_{t_l+6:T} = \mathbf{v}, I_0 = a), \end{aligned} \tag{9}$$

$$\tag{10}$$

we define $\mathcal{I} = \mathcal{I}_{\text{init}} \cup \mathcal{I}_{\text{init, lock}}$, where

$$\mathcal{I}_{\text{init}} = \{\iota_{\mathbf{v}, a} \mid (\mathbf{v}, a) \in [0, 1]^4\}, \tag{11}$$

$$\mathcal{I}_{\text{init, lock}} = \{\iota_{\mathbf{v}, a, t_l} \mid (\mathbf{v}, a, t_l) \in [0, 1]^4 \times \llbracket 5, 10 \rrbracket\}. \tag{12}$$

Table 1: Metrics for interventionally (**I**) and observationally (**O**) trained surrogates on interventional (**I'**) and observational (**O'**) test set (median^{third quantile}/_{first quantile} from 5 repeats). Bold indicates best performance.

Test	Model Train	LRNN		LODE-RNN		LODE	
		I	O	I	O	I	O
I'	AMSE ($\times 10^{-1}$)	3.475 _{3.405} ^{3.910}	49.44 _{46.66} ^{52.61}	3.350 _{3.179} ^{3.410}	18.47 _{17.12} ^{21.91}	8.150 _{8.058} ^{8.242}	22.39 _{22.14} ^{22.65}
	ANLL ($\times 10^3$)	2.091 _{2.030} ^{2.164}	21.77 _{20.13} ^{22.93}	1.987 _{1.980} ^{1.990}	8.396 _{8.269} ^{9.885}	4.008 _{3.999} ^{4.017}	10.03 _{9.909} ^{10.14}
O'	AMSE ($\times 10^{-1}$)	4.127 _{4.105} ^{4.259}	2.945 _{2.623} ^{3.155}	3.592 _{3.538} ^{3.681}	2.523 _{2.164} ^{2.783}	18.42 _{18.14} ^{18.71}	4.361 _{4.321} ^{4.401}
	ANLL ($\times 10^3$)	2.220 _{2.156} ^{2.231}	1.641 _{1.431} ^{1.709}	1.855 _{1.850} ^{1.968}	1.429 _{1.267} ^{1.528}	7.629 _{7.517} ^{7.741}	2.151 _{2.131} ^{2.170}

The first of these is a subset of interventions that fix the initial proportion of infected individuals in the agent-based simulator, as well as its parameter values. The second subset of interventions is the set of interventions that fix (a) the initial proportion of infected individuals in the ABM, (b) the values of the ABM’s parameters before, during, and beyond a lockdown beginning at time $t_l \in \llbracket 5, 10 \rrbracket$ with duration equal to 5 time steps, and (c) the value of t_l . Similarly defining

$$\iota'_{\tilde{\mathbf{v}}, \tilde{a}} = \text{do} \left(\tilde{\boldsymbol{\theta}}_{1:T} = \tilde{\mathbf{v}}, \tilde{I}_0 = \tilde{a} \right), \quad (13)$$

$$\begin{aligned} \iota'_{\tilde{\mathbf{v}}, \tilde{a}, \tilde{t}_l} &= \text{do} \left(\tilde{\boldsymbol{\theta}}_{1:\tilde{t}_l-1} = \tilde{\mathbf{v}}, \tilde{\boldsymbol{\theta}}_{\tilde{t}_l:\tilde{t}_l+5} = \tilde{\mathbf{v}} \odot (0, 1, 1), \right. \\ &\quad \left. \tilde{\boldsymbol{\theta}}_{\tilde{t}_l+6:T} = \tilde{\mathbf{v}}, \tilde{I}_0 = \tilde{a} \right), \end{aligned} \quad (14)$$

we furthermore define the intervention set $\mathcal{I}' = \mathcal{I}'_{\text{init}} \cup \mathcal{I}'_{\text{init, lock}}$ for the macromodels, where

$$\mathcal{I}'_{\text{init}} = \{ \iota'_{\tilde{\mathbf{v}}, \tilde{a}} \mid (\tilde{\mathbf{v}}, \tilde{a}) \in \mathbb{R}_{\geq 0}^3 \times [0, 1] \}, \quad (15)$$

$$\begin{aligned} \mathcal{I}'_{\text{init, lock}} &= \{ \iota'_{\tilde{\mathbf{v}}, \tilde{a}, \tilde{t}_l} \mid \\ &\quad (\tilde{\mathbf{v}}, \tilde{a}, \tilde{t}_l) \in \mathbb{R}_{\geq 0}^3 \times [0, 1] \times \llbracket 5, 10 \rrbracket \}. \end{aligned} \quad (16)$$

The map τ is taken to map: $\boldsymbol{\theta}_t$ identically to $\tilde{\boldsymbol{\theta}}_t$ for each $t \in \llbracket 1, T \rrbracket$; the microstate \mathbf{x}_t of the ABM at each time step to the $\tilde{\mathbf{y}}_t$ through an aggregation map that counts the number of agents in \mathbf{x}_t in each of the three possible states (susceptible, infectious, and recovered); and the initial proportion I_0 of infected agents in the ABM identically to \tilde{I}_0 . The map ω^ϕ is taken to act as

$$\omega^\phi : \iota_{\mathbf{v}, a} \mapsto \iota'_{f^\phi(\mathbf{v}), a} \quad , \quad \iota_{\mathbf{v}, a, t_l} \mapsto \iota'_{f^\phi(\mathbf{v}), a, t_l} \quad (17)$$

for a neural network $f^\phi : [0, 1]^3 \rightarrow \mathbb{R}_{\geq 0}^3$.

5.2 The Benefits of Training with Interventional Data

To explore the benefits of training a surrogate macromodel with interventional consistency in mind, we jointly learn the parameters ϕ, ψ of the surrogates and the map ω^ϕ described above in two different ways¹:

Observationally trained surrogates The first approach entails training the surrogate models with η taken to be a uniform distribution $\mathcal{U}(\mathcal{I}_{\text{init}})$ over $\mathcal{I}_{\text{init}}$.

Interventionally trained surrogates This second approach entails training with η instead taken to be a uniform distribution $\mathcal{U}(\mathcal{I})$ over \mathcal{I} .

We indicate the two approaches to training the surrogates with, respectively, bold uppercase **O** and **I**. Details of the training procedure and neural network architectures are provided in Appendix E. We assess the interventional consistency of the surrogates resulting from these two training schemes by computing error metrics on a hold-out test dataset $\mathbf{I}' = \{ \mathbf{y}_{0:T}^{(r')} \}_{r'=1}^{R'}$ of size $R' = 1000$, generated for each $r' \in \llbracket 1, R' \rrbracket$ as:

$$\iota^{(r')} \sim \eta = \mathcal{U}(\mathcal{I}), \quad \mathbf{y}_{0:T}^{(r')} \sim \tau_{\#} \left(\mathbb{P}_{\mathcal{M}_{\iota^{(r')}}} \right). \quad (18)$$

Specifically, we inspect two error metrics with respect to this hold-out set, for which lower values are better:

¹“Observationally” and “interventionally” are misnomers: both are trained interventional, but differ in the interventional distribution η used to train. We nonetheless retain this naming scheme since it reflects the fact that one set contains the policy “interventions” of interest while the other does not intervene during program execution.

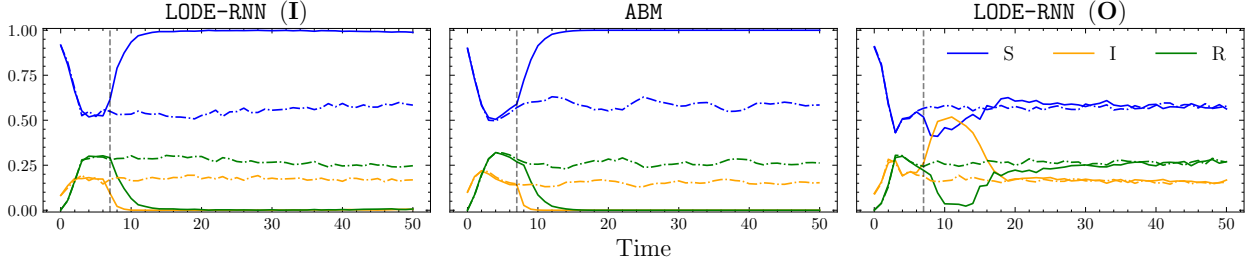


Figure 5: Example of trajectories from the ABM (middle) and the LODE-RNN trained on interventional (left) and observational (right) data. A lockdown is imposed at the dashed vertical line. Solid lines show trajectories under the lockdown, while dot-dash lines show trajectories without lockdown. The effectiveness of the lockdown in reducing infections is vastly underestimated in the observationally trained surrogate, while the interventionally trained surrogate accurately predicts that the lockdown will effectively reduce the spread of infection.

The average mean squared error between trajectories $\tilde{\mathbf{y}}_{0:T}^{(r')}$ from the surrogates and the $\mathbf{y}_{0:T}^{(r')}$, i.e.,

$$\text{AMSE} = \frac{1}{N^2 R'} \sum_{r'=1}^{R'} \frac{1}{T+1} \sum_{t=0}^T \left\| \tilde{\mathbf{y}}_t^{(r')} - \mathbf{y}_t^{(r')} \right\|^2 \quad (19)$$

where $\tilde{\mathbf{y}}_{0:T}^{(r')} \sim \mathbb{P}_{\mathcal{M}_{\omega, \phi^*}^{\psi^*}(\iota^{(r')})}$ for $r' \in \llbracket 1, R' \rrbracket$.

The average negative log-likelihood of this test data under the likelihood of the learned surrogates, i.e.

$$\text{ANLL} = \frac{1}{R'} \sum_{r'=1}^{R'} -\log q_{\omega, \phi^*}^{\psi^*}(\iota^{(r')}) (\mathbf{y}_{0:T}^{(r')}), \quad (20)$$

Observational consistency is checked on a different hold-out test set \mathbf{O}' , generated by taking $\eta = \mathcal{U}(\mathcal{I}_{\text{init}})$.

Table 1 shows the values of these performance metrics evaluated on \mathbf{I}' and \mathbf{O}' for all surrogate families and training schemes. We observe that far lower values of the error metrics are obtained by the interventionally, rather than observationally, trained surrogates when assessing interventional consistency. This suggests that training on interventional data can result in more accurate predictions about the effect of interventions in the ABM, and that data drawn from the relevant interventional distributions associated with the ABM should be included during training if the policy-maker intends to perform policy experiments with the surrogate. Not surprisingly, we also report a minor drop in observational consistency when training with data from the combined intervention set \mathcal{I} instead of $\mathcal{I}_{\text{init}}$, which can be explained by the overfit of the observationally-trained model on the observational test set. We also observe that the LODE-RNN – which combines the “mechanistic” SIRS ODE with a flexible RNN – achieves the best interventional and observational consistencies of the three families of surrogates, suggesting that such hybrid approaches to constructing flexible surrogates are promising choices under our proposed method.

In Figure 5, we show an example of a possible negative consequence of failing to train a surrogate on data drawn from the appropriate ABM interventional distributions. In the middle panel, we show the change in the ABM trajectory induced by imposing a lockdown at time $t_l = 7$, while in the left (resp. right) panel we show corresponding trajectories from the interventionally (resp. observationally) trained surrogates under the equivalent intervention learned through our training procedure. While the interventionally trained LODE-RNN correctly predicts that the lockdown effectively impedes the spread of the disease in the ABM, the observationally trained surrogate predicts that the lockdown will temporarily *increase* infections, before approximately reverting to the behaviour of the model without a lockdown. The use of such a surrogate model in policy experiments when limited computational resources do not permit use of the accurate, high-fidelity ABM of the underlying complex system may therefore have misdirected policy-makers towards suboptimal policies and away from effective interventions.

6 Related Work

Surrogates are frequently used in agent-based modelling. Increasingly, modern approaches for constructing surrogates rely on established machine learning methods such as random forests (Lamperti et al., 2018; De Leeuw et al., 2023),

artificial neural networks (Anirudh et al., 2022; De Leeuw et al., 2023), support vector machines (ten Broeke et al., 2021), kriging (Salle and Yıldızoğlu, 2014), and mixture density networks (MDNs) (Platt, 2022). Our experiments also rely on established machine learning methods to construct surrogates; in particular, our LRNN surrogate family resembles that of Platt (2022), in which MDNs are used to approximate the transition density for ABMs. However, surrogates in agent-based modelling are typically used to expedite simulation-based inference, and their *causal/interventional* consistency with respect to the ABM and policy interventions of interest is not generally considered. In contrast to prior work, we explicitly detail the causal structure of our surrogates and their causal relation to the underlying ABM via causal abstraction, broadening the scope of surrogate modelling to permit policy experimentation with the surrogate.

The notions of causal abstraction and exact transformation were originally introduced by Rubenstein et al. (2017). This seminal work was extended in Beckers and Halpern (2019), where stricter definitions of causal abstraction were proposed, and in Beckers et al. (2020), where approximate relationships of abstraction are introduced to account for uncertainty and simplification. The notion of abstraction found practical application in Geiger et al. (2021) for learning interpretable neural networks. An alternative category-theoretical definition of abstraction was developed by Rischel and Weichwald (2021), and used for learning abstractions to transfer data between models at different levels of abstraction in Zennaro et al. (2023a).

7 Conclusion

Summarising, we have proposed a rigorous framework for learning interventionally consistent surrogates for ABMs, formalised through the notion of casual abstraction. Our experiments highlight the efficacy of our framework against purely observational methods that do not train on interventional data. To the best of our knowledge, our framework is the first application of causal abstraction within the ABM literature.

In this sense, our work is a first step in formally applying the tools of casual abstraction, and causal inference more generally, to agent-based models. As illustrated in this work, ABMs implicitly define causal models for underlying real world systems, and their use in modelling *what-if* scenarios is a causal problem rather than a purely statistical one. Hence, it is natural to conjecture that the theory of causality will play a key role in formalising and addressing many other open problems within the ABM community.

Acknowledgements

This research was supported by a UKRI AI World Leading Researcher Fellowship awarded to Wooldridge (grant EP/W002949/1). **MW** and **AC** acknowledge funding from Trustworthy AI - Integrating Learning, Optimisation and Reasoning (TAILOR), a project funded by European Union Horizon2020 research and innovation program under Grant Agreement 952215. **YF**: This scientific paper was supported by the Onassis Foundation - Scholarship ID: F ZR 063-1/2021-2022. **TD**: Acknowledges support from a UKRI Turing AI acceleration Fellowship [EP/V02678X/1]. The authors would also like to acknowledge the University of Warwick Research Technology Platform (RTP) for assistance in the research described in this paper and the EPSRC platform for ensemble computing “Sulis” [EP/T022108/1].

References

- Rafa Baptista, J Doyne Farmer, Marc Hinterschweiger, Katie Low, Daniel Tang, and Arzu Uluc. Staff Working Paper No. 619 Macropprudential policy in an agent-based model of the UK housing market. *Bank of England*, 2016.
- Cliff C. Kerr, Robyn M. Stuart, Dina Mistry, Romesh G. Abeysuriya, Katherine Rosenfeld, Gregory R. Hart, Rafael C. Núñez, Jamie A. Cohen, Prashanth Selvaraj, Brittany Hagedorn, Lauren George, Michał Jastrzębski, Amanda S. Izzo, Greer Fowler, Anna Palmer, Dominic Delpert, Nick Scott, Sherrie L. Kelly, Caroline S. Bennette, Bradley G. Wagner, Stewart T. Chang, Assaf P. Oron, Edward A. Wenger, Jasmina Panovska-Griffiths, Michael Famulare, and Daniel J. Klein. Covasim: An agent-based model of covid-19 dynamics and interventions. *PLOS Computational Biology*, 17(7): 1–32, 07 2021. doi:10.1371/journal.pcbi.1009149. URL <https://doi.org/10.1371/journal.pcbi.1009149>.
- Rama Cont. Volatility clustering in financial markets: empirical facts and agent-based models. *Long memory in economics*, pages 289–309, 2007.
- AG Haldane and AE Turrell. An interdisciplinary model for macroeconomics. *Oxford Review of Economic Policy*, 34 (1-2):219–251, 2018.
- Sander Beckers and Joseph Y Halpern. Abstracting causal models. In *Proceedings of the AAAI Conference on Artificial Intelligence*, volume 33, pages 2678–2685, 2019.

- Fabio Massimo Zennaro, Máté Drávucz, Geanina Apachitei, W. Dhammika Widanage, and Theodoros Damoulas. Jointly learning consistent causal abstractions over multiple interventional distributions. In *2nd Conference on Causal Learning and Reasoning*, 2023a. URL <https://openreview.net/forum?id=RNs7aMS6zDq>.
- Judea Pearl. *Causality*. Cambridge University Press, 2009.
- Paul K Rubenstein, Sebastian Weichwald, Stephan Bongers, Joris M Mooij, Dominik Janzing, Moritz Grosse-Wentrup, and Bernhard Schölkopf. Causal consistency of structural equation models. In *33rd Conference on Uncertainty in Artificial Intelligence (UAI 2017)*, pages 808–817. Curran Associates, Inc., 2017.
- Sander Beckers, Frederick Eberhardt, and Joseph Y Halpern. Approximate causal abstractions. In *Uncertainty in Artificial Intelligence*, pages 606–615. PMLR, 2020.
- Yulia Rubanova, Ricky TQ Chen, and David K Duvenaud. Latent ordinary differential equations for irregularly-sampled time series. *Advances in neural information processing systems*, 32, 2019.
- Francesco Lamperti, Andrea Roventini, and Amir Sani. Agent-based model calibration using machine learning surrogates. *Journal of Economic Dynamics and Control*, 90:366–389, 2018. ISSN 0165-1889. doi:<https://doi.org/10.1016/j.jedc.2018.03.011>. URL <https://www.sciencedirect.com/science/article/pii/S0165188918301088>.
- Benyamin De Leeuw, S. Sahand Mohammadi Ziabari, and Alexei Sharpanskykh. Surrogate modeling of agent-based airport terminal operations. In Fabian Lorig and Emma Norling, editors, *Multi-Agent-Based Simulation XXIII*, pages 82–94, Cham, 2023. Springer International Publishing. ISBN 978-3-031-22947-3.
- Rushil Anirudh, Jayaraman J. Thiagarajan, Peer-Timo Bremer, Timothy Germann, Sara Del Valle, and Frederick Streit. Accurate calibration of agent-based epidemiological models with neural network surrogates. In Peng Xu, Tingting Zhu, Pengkai Zhu, David A. Clifton, Danielle Belgrave, and Yuanting Zhang, editors, *Proceedings of the 1st Workshop on Healthcare AI and COVID-19, ICML 2022*, volume 184 of *Proceedings of Machine Learning Research*, pages 54–62. PMLR, 22 Jul 2022. URL <https://proceedings.mlr.press/v184/anirudh22a.html>.
- Guus ten Broeke, George van Voorn, Arend Ligtenberg, and Jaap Molenaar. The use of surrogate models to analyse agent-based models. *Journal of Artificial Societies and Social Simulation*, 24(2):3, 2021. ISSN 1460-7425. doi:10.18564/jasss.4530. URL <http://jasss.soc.surrey.ac.uk/24/2/3.html>.
- Isabelle Salle and Murat Yıldızoğlu. Efficient sampling and meta-modeling for computational economic models. *Computational Economics*, 44(4):507–536, Dec 2014. ISSN 1572-9974. doi:10.1007/s10614-013-9406-7. URL <https://doi.org/10.1007/s10614-013-9406-7>.
- Donovan Platt. Bayesian estimation of economic simulation models using neural networks. *Computational Economics*, 59(2):599–650, 2022.
- Atticus Geiger, Hanson Lu, Thomas Icard, and Christopher Potts. Causal abstractions of neural networks. *Advances in Neural Information Processing Systems*, 34:9574–9586, 2021.
- Eigil F Rischel and Sebastian Weichwald. Compositional abstraction error and a category of causal models. In *Uncertainty in Artificial Intelligence*, pages 1013–1023. PMLR, 2021.
- Jonas Peters, Dominik Janzing, and Bernhard Schölkopf. *Elements of causal inference: Foundations and learning algorithms*. MIT Press, 2017.
- Peter Spirtes, Clark N Glymour, and Richard Scheines. *Causation, prediction, and search*. MIT press, 2000.
- Fabio Massimo Zennaro, Paolo Turrini, and Theo Damoulas. Quantifying consistency and information loss for causal abstraction learning. In *Proceedings of the Thirtieth International Conference on Artificial Intelligence*, 2023b.
- Eigil Fjeldgren Rischel. The category theory of causal models. Master’s thesis, University of Copenhagen, 2020.
- Joel Dyer, Patrick Cannon, J Doyne Farmer, and Sebastian Schmon. Black-box Bayesian inference for economic agent-based models. *arXiv preprint arXiv:2202.00625*, 2022a.
- Joel Dyer, Patrick Cannon, J Doyne Farmer, and Sebastian M Schmon. Calibrating Agent-based Models to Microdata with Graph Neural Networks. In *ICML 2022 Workshop AI for Agent-Based Modelling*, 2022b.
- Annalisa Fabretti. On the problem of calibrating an agent based model for financial markets. *Journal of Economic Interaction and Coordination*, 8(2):277–293, Oct 2013. ISSN 1860-7128. doi:10.1007/s11403-012-0096-3. URL <https://doi.org/10.1007/s11403-012-0096-3>.
- M. Gilli and P. Winker. A global optimization heuristic for estimating agent based models. *Computational Statistics and Data Analysis*, 42(3):299–312, 2003. ISSN 0167-9473. doi:[https://doi.org/10.1016/S0167-9473\(02\)00214-1](https://doi.org/10.1016/S0167-9473(02)00214-1). URL <https://www.sciencedirect.com/science/article/pii/S0167947302002141>. Computational Econometrics.

- Donovan Platt and Tim Gebbie. Can agent-based models probe market microstructure? *Physica A: Statistical Mechanics and its Applications*, 503:1092–1106, 2018. ISSN 0378-4371. doi:<https://doi.org/10.1016/j.physa.2018.08.055>. URL <https://www.sciencedirect.com/science/article/pii/S0378437118309956>.
- Jakob Grazzini and Matteo Richiardi. Estimation of ergodic agent-based models by simulated minimum distance. *Journal of Economic Dynamics and Control*, 51:148–165, 2015. ISSN 0165-1889. doi:<https://doi.org/10.1016/j.jedc.2014.10.006>. URL <https://www.sciencedirect.com/science/article/pii/S0165188914002814>.
- Francesco Lamperti. An information theoretic criterion for empirical validation of simulation models. *Econometrics and Statistics*, 5:83–106, 2018. ISSN 2452-3062. doi:<https://doi.org/10.1016/j.ecosta.2017.01.006>. URL <https://www.sciencedirect.com/science/article/pii/S2452306217300084>.
- Sylvain Barde and Sander van Der Hoog. An empirical validation protocol for large-scale agent-based models. *Bielefeld working papers in economics and management*, 2017.
- Donovan Platt. A comparison of economic agent-based model calibration methods. *Journal of Economic Dynamics and Control*, 113:103859, 2020. ISSN 0165-1889. doi:<https://doi.org/10.1016/j.jedc.2020.103859>. URL <https://www.sciencedirect.com/science/article/pii/S0165188920300294>.
- Joel Dyer. *Likelihood-free Bayesian inference for dynamic, stochastic simulators in the social sciences*. PhD thesis, University of Oxford, 2022.
- Carles Gelada, Saurabh Kumar, Jacob Buckman, Ofir Nachum, and Marc G. Bellemare. DeepMDP: Learning continuous latent space models for representation learning. In Kamalika Chaudhuri and Ruslan Salakhutdinov, editors, *Proceedings of the 36th International Conference on Machine Learning*, volume 97 of *Proceedings of Machine Learning Research*, pages 2170–2179. PMLR, 09–15 Jun 2019. URL <https://proceedings.mlr.press/v97/gelada19a.html>.
- Florent Delgrange, Ann Nowé, and Guillermo A. Pérez. Distillation of RL Policies with Formal Guarantees via Variational Abstraction of Markov Decision Processes. *Proceedings of the AAAI Conference on Artificial Intelligence*, 36(6):6497–6505, Jun. 2022. doi:10.1609/aaai.v36i6.20602. URL <https://ojs.aaai.org/index.php/AAAI/article/view/20602>.
- Christopher Rackauckas, Yingbo Ma, Julius Martensen, Collin Warner, Kirill Zubov, Rohit Supekar, Dominic Skinner, Ali Ramadhan, and Alan Edelman. Universal differential equations for scientific machine learning, 2021.
- Diederik P Kingma and Jimmy Ba. Adam: A method for stochastic optimization. *arXiv preprint arXiv:1412.6980*, 2014.

Supplementary Material: Interventionally Consistent Surrogates for Agent-based Simulators

A ASSUMPTIONS UNDERLYING MARKOVIAN SCMS

Definition 1 implies the standard assumptions of (i) *acyclicity* of the DAG $\mathcal{G}_{\mathcal{M}}$ and (ii) *causal sufficiency*, meaning that there are no unobserved confounders (Pearl, 2009; Peters et al., 2017). These two assumptions entail that our SCMs are Markovian.

We also assume *faithfulness*, guaranteeing that independencies in the data are captured in the graphical model Spirtes et al. (2000).

B OTHER NOTIONS OF ABSTRACTION ERROR

As discussed in Section 3, Definition 4 is closely related to the notion of abstraction error introduced by Beckers et al. (2020). In contrast to Definition 4, Beckers et al. (2020) employ a maximum over the intervention set \mathcal{I} instead of an expectation. Hence, the abstraction error introduced by Beckers et al. (2020) may be viewed as a worst-case version of Definition 4.

In addition, Beckers and Halpern (2019) assume the intervention map ω can be implicitly defined by the map τ , and require the abstraction map τ to be consistent. That is, the image of \mathcal{I} under the intervention map induced by τ must equal \mathcal{I}' . Since we do not couple the maps τ and ω we enforce no such condition. Additionally, Beckers et al. (2020) enforce surjectivity of τ . Since this makes no practical difference in a surrogate’s use in downstream tasks, we dispense with this assumption.

Alternative notions of abstraction error have been introduced by Zennaro et al. (2023b), building upon the notion of exact transformations introduced by Rischel (2020). We conjecture that an analogous version of our framework may be developed for this setting, wherein the aggregation function over the intervention set is again chosen to be an expectation over an interventional distribution η instead of a maximum, and we leave this as a direction for future work.

C ADDITIONAL RELATED WORK

Surrogate modelling of ABMs is closely related to the problem of ABM calibration. Calibration involves tuning (a distribution over) ABM parameters so that data generated by the ABM matches that generated by the real world system being modelled (Dyer et al., 2022a,b). Analogously, surrogate modelling consists of tuning surrogate parameters so that data generated by the surrogate matches data generated by the corresponding ABM. Hence, a number of methods for calibration can naturally be applied to learn surrogates. Several calibration techniques and metrics have been proposed in the literature, including the method of simulated moments (Fabretti, 2013; Gilli and Winker, 2003; Platt and Gebbie, 2018), simulated minimum distance (Grazzini and Richiardi, 2015), generalised subtracted L-divergence (Lamperti, 2018) and Markov information criterion (Barde and van Der Hoog, 2017). We refer the reader to Platt (2020); Dyer (2022) for thorough surveys. Unlike our framework, these techniques and metrics do not explicitly account for interventional consistency.

More generally, our framework bears many similarities to latent space modelling of Markov decision processes (MDPs) (Gelada et al., 2019), wherein one attempts to learn a smaller latent MDP from a target MDP, whose size precludes its use in downstream tasks. For downstream tasks such as formal verification of policies, Delgrange et al. (2022) employs the bisimulation metric to measure the consistency of their latent MDPs with respect to the target. Abstraction error plays an analogous role in our framework, where the original MDP corresponds to the ABM, and the latent MDP the surrogate. Likewise, the surrogates we propose in Section 5 are implicitly connected to the scientific modelling framework of Rackauckas et al. (2021), who embed prior information regarding system dynamics into systems of universal differential equations represented by neural architectures such as neural ODEs. We embed the underlying dynamics of the classical SIRS ODE into several surrogates in an attempt to learn better causal abstractions.

D PROOFS

D.1 Proof of Proposition 1

Proof. By non-negativity of the divergence d we have $d\left(\tau_{\#}(\mathbb{P}_{\mathcal{M}_\iota}, \mathbb{P}_{\mathcal{M}'_{\omega(\iota)}})\right) \geq 0$ for all $\iota \in \mathcal{I}$. Hence $d_{\tau, \omega}(\mathcal{M}, \mathcal{M}')$ corresponds to an expectation over a non-negative random variable. Since this expectation is equal to zero, we conclude that $d\left(\tau_{\#}(\mathbb{P}_{\mathcal{M}_\iota}, \mathbb{P}_{\mathcal{M}'_{\omega(\iota)}})\right) = 0$ almost surely with respect to the distribution η . Positivity of the divergence d then implies that $\tau_{\#}(\mathbb{P}_{\mathcal{M}_\iota}) = \mathbb{P}_{\mathcal{M}'_{\omega(\iota)}}$ almost surely with respect to the distribution η . \square

D.2 Proof of Proposition 2

Proof. Using Markov's inequality and the fact that $d_{\tau, \omega \phi}(\mathcal{M}, \mathcal{M}^\psi) = \mathbb{E}_{\iota \sim \eta} \left[d\left(\tau_{\#}(\mathbb{P}_{\mathcal{M}_\iota}, \mathbb{P}_{\mathcal{M}^\psi_{\omega \phi(\iota)}})\right) \right]$:

$$\mathbb{P}_\eta \left(d\left(\tau_{\#}(\mathbb{P}_{\mathcal{M}_\iota} \parallel \mathbb{P}_{\mathcal{M}^\psi_{\omega \phi(\iota)}})\right) \geq \epsilon \right) \leq \frac{d_{\tau, \omega \phi}(\mathcal{M}, \mathcal{M}^\psi)}{\epsilon}.$$

Since we have a finite domain, the likelihood functions associated with (a) the pushforward measure of the ABM under τ and (b) the surrogate macromodel can be written as probability mass functions, whose logarithms are non-positive. Since we have assumed $\mathbb{P}_{\mathcal{M}^\psi_{\omega \phi(\iota)}} \ll \tau_{\#}(\mathbb{P}_{\mathcal{M}_\iota})$, we have that $0 \leq -\log q_{\omega \phi(\iota)}^\psi(\mathbf{Y}) < \infty$ for any $\mathbf{Y} \sim \tau_{\#}(\mathbb{P}_{\mathcal{M}_\iota})$, and therefore

$$0 \leq \mathbb{E}_{\iota \sim \eta} [\mathbf{CE}_\iota] < \infty. \quad (21)$$

We also have that

$$-\mathbb{H}_{\tau_{\#}(\mathbb{P}_{\mathcal{M}_\iota})} \leq 0 \Rightarrow \mathbb{E}_{\iota \sim \eta} [-\mathbb{H}_{\tau_{\#}(\mathbb{P}_{\mathcal{M}_\iota})}] \leq 0, \quad (22)$$

where $\mathbb{H}_{\tau_{\#}(\mathbb{P}_{\mathcal{M}_\iota})}$ is the entropy of the probability mass function associated with $\tau_{\#}(\mathbb{P}_{\mathcal{M}_\iota})$, and that

$$d\left(\tau_{\#}(\mathbb{P}_{\mathcal{M}_\iota}, \mathbb{P}_{\mathcal{M}^\psi_{\omega \phi(\iota)}})\right) = -\mathbb{H}_{\tau_{\#}(\mathbb{P}_{\mathcal{M}_\iota})} + \mathbf{CE}_\iota \geq 0 \quad (23)$$

$$\Rightarrow d_{\tau, \omega \phi}(\mathcal{M}, \mathcal{M}^\psi) = \mathbb{E}_{\iota \sim \eta} [-\mathbb{H}_{\tau_{\#}(\mathbb{P}_{\mathcal{M}_\iota})}] + \mathbb{E}_{\iota \sim \eta} [\mathbf{CE}_\iota] \leq \mathbb{E}_{\iota \sim \eta} [\mathbf{CE}_\iota]. \quad (24)$$

Hence

$$\mathbb{P}_\eta \left(d\left(\tau_{\#}(\mathbb{P}_{\mathcal{M}_\iota} \parallel \mathbb{P}_{\mathcal{M}^\psi_{\omega \phi(\iota)}})\right) \geq \epsilon \right) \leq \frac{\mathbb{E}_{\iota \sim \eta} [\mathbf{CE}_\iota]}{\epsilon}. \quad (25)$$

\square

E FURTHER EXPERIMENTAL DETAILS

As described in the main text, the three surrogate families we consider have SCMs whose corresponding DAGs can be drawn as in Figure 4. In this section, we fully specify the corresponding SCM for each surrogate. Furthermore, for each surrogate, we provide details on the procedure used to train the parameters ψ and ϕ , which respectively describe the structural equations of each SCM and their corresponding intervention map ω .

E.1 The LODE Surrogate Family

To construct a set \mathfrak{M} of probabilistic SCMs, we define a latent neural ordinary differential equation (LNODE) based on the classical SIRS ODE system. The SIRS ODE system takes the form

$$\begin{aligned} \frac{d\tilde{S}_t}{dt} &= \tilde{\gamma}_t \tilde{R}_t - \tilde{\alpha}_t \tilde{I}_t \tilde{S}_t, & \frac{d\tilde{I}_t}{dt} &= \tilde{\alpha}_t \tilde{I}_t \tilde{S}_t - \tilde{\beta}_t \tilde{I}_t, \\ \frac{d\tilde{R}_t}{dt} &= \tilde{\beta}_t \tilde{I}_t - \tilde{\gamma}_t \tilde{R}_t, \end{aligned} \quad (26)$$

where $\tilde{\theta}_t = (\tilde{\alpha}_t, \tilde{\beta}_t, \tilde{\gamma}_t) \in \mathbb{R}_{>0}^3$ are the ODE parameters and $\mathbf{z}_t = (\tilde{S}_t, \tilde{I}_t, \tilde{R}_t) \in \mathcal{S} \forall t \in [0, T]$ is the ODE state, where \mathcal{S} is the two-simplex. Note that \mathbf{z}_t represents the proportion of susceptible, infected and recovered individuals in the population according the SIRS ODE. Whilst the parameters $\tilde{\theta}_t$ may change over time – which will permit the

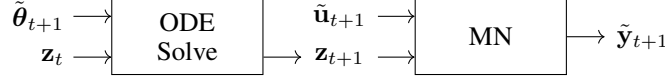


Figure 6: A schematic representation of the LODE surrogate family for a single time step. First, the output of the SIRS ODE for the next time step, \mathbf{z}_{t+1} , is computed via ODESolve. Then, \mathbf{z}_{t+1} serves as the logits for a multinomial distribution from which $\tilde{\mathbf{y}}_t$ is sampled. This sampling procedure is denoted by MN in the diagram. The exogenous variables required to reparameterise the multinomial distribution during sampling are denoted by $\tilde{\mathbf{u}}_t$.

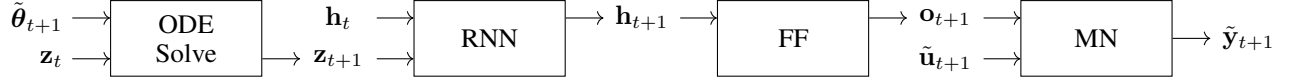


Figure 7: A schematic representation of the LODE-RNN surrogate family for a single time step. First, the output of the SIRS ODE for the next time step, \mathbf{z}_{t+1} , is computed via ODESolve. Then, \mathbf{z}_{t+1} is passed through to the hidden state of a recurrent neural network (denoted by RNN in the diagram) that updates its hidden state from \mathbf{h}_t to \mathbf{h}_{t+1} . The updated hidden state is passed to a feedforward neural network (denoted by FF in the diagram), which computes the logits \mathbf{o}_{t+1} for a multinomial distribution from which $\tilde{\mathbf{y}}_{t+1}$ is sampled.

experimenter to intervene on the values of the parameters at different time steps – we assume the simplest case of assigning the same vector $\tilde{\mathbf{v}} \in \mathbb{R}_{\geq 0}^3$ to all $\tilde{\theta}_t$ when no interventions are applied:

$$\tilde{\theta}_t = \tilde{\mathbf{v}}, \quad \forall t \in [0, T]. \quad (27)$$

In other words, Equation (27) describes the structural equation $\tilde{f}_{\tilde{\theta}_t}$ for $\tilde{\theta}_t$. Practically speaking, the choice of $\tilde{\mathbf{v}}$ is inconsequential, as we can model any change to $\tilde{\theta}_t$ as an intervention. Given $\tilde{\theta}_t$, the ODE state \mathbf{z}_t evolves according to the following rule:

$$\mathbf{z}_t = \text{ODESolve}(\mathbf{z}_{t-1}, \tilde{\theta}_t), \quad t \in \llbracket 1, T \rrbracket, \quad (28)$$

where ODESolve denotes numerical integration of System 26 between times $t - 1$ and t . In our experiments, we compute this using a Euler scheme with step size $\Delta t = 1$. The initial state of the ODE is taken to be $\mathbf{z}_0 = (1 - \tilde{I}_0, \tilde{I}_0, 0)$. One may change the initial state \mathbf{z}_0 through interventions on \tilde{I}_0 , which is modelled as an endogenous variable.

Given \mathbf{z}_t , we draw the endogenous variables $\tilde{\mathbf{y}}_t$ from a multinomial distribution whose class probabilities are given by \mathbf{z}_t . Whilst \mathbf{z}_t represents the percentage of susceptible, infected, and recovered individuals predicted by the SIR ODE, $\tilde{\mathbf{y}}_t$ represents the actual counts observed by the experimenter. We write $\tilde{f}_{\tilde{\mathbf{y}}_t}(\tilde{I}_0, \tilde{\theta}_{1:t}, \tilde{\mathbf{u}}_t)$ to denote the structural function associated with $\tilde{\mathbf{y}}_t$, where the dependence on \tilde{I}_0 and $\tilde{\theta}_{t'}$ for $t' \leq t$ is mediated by the trajectory followed by the $\mathbf{z}_{t'}$ for $t' \leq t$, and $\tilde{\mathbf{u}}_t$ are the exogenous random variables required to reparameterise the multinomial sampling procedure on each time step.

Note that $\psi = \emptyset$ for this family of surrogates, and hence \mathfrak{M} is a singleton. For the function f^ϕ comprising the intervention map ω^ϕ , we take a feedforward network with layer sizes 3, 32, 64, 64, 64, 32, 3. A ReLU activation is applied after each hidden layer, and a sigmoid activation is applied to the final output layer. The sigmoid activation function ensures that the predicted intervention vector $f^\phi(\mathbf{v})$ on the parameters of the LODE has all of its components in the range $[0, 1]$, which is suitable when forward simulating the ODE with an Euler scheme with $\Delta t = 1$. This feedforward network consists of 12,739 trainable parameters.

E.2 The LODE-RNN Surrogate Family

This surrogate family closely mimics the LODE family described above, and differs only in that the class *logits* of the multinomial distributions are instead indexed by the output of a feedforward network – with layer sizes 32, 32, 64, 32, 16, 3, where all hidden layers are followed by a ReLU activation function – which maps from the hidden state $\mathbf{h}_t \in \mathbb{R}^{32}$ of a GRU recurrent network that is passed over the trajectory $\mathbf{z}_{0:T}$ generated from the SIRS ODE (forward simulated as described above). The combined action of the ODE solver, the GRU-feedforward networks, and the reparameterisation of sampling from the multinomial distributions, define the structural equations $\tilde{f}_{\tilde{\mathbf{y}}_t} : (\tilde{I}_0, \tilde{\theta}_{1:t}, \tilde{\mathbf{u}}_t) \mapsto \tilde{\mathbf{y}}_t$ for each $t \in \llbracket 1, T \rrbracket$.

For this model, ψ is the collection of trainable parameters comprising these GRU and feedforward networks. For f^ϕ , we use a feedforward network with layer sizes 3, 32, 64, 32, 3, where a ReLU activation is applied after all hidden layers and a sigmoid activation is applied after the final layer. Thus, the total number of trainable parameters from ψ and ϕ combined is 13,798.

E.3 The LRNN Surrogate Family

This surrogate family makes no use of the SIRS ODE model. Instead, the logits of the multinomial distributions for $t \in \llbracket 1, T \rrbracket$ are indexed by the outputs $(\mathbf{o}_1, \dots, \mathbf{o}_T)$, $\mathbf{o}_t \in \mathbb{R}^3$ of a feedforward network – with layer sizes 32, 32, 64, 32, 16, 3, and where all hidden layers are followed by a ReLU activation function – that maps from the hidden state $\mathbf{h}_t \in \mathbb{R}^{32}$ of a GRU recurrent network which is passed over the sequence $\tilde{\boldsymbol{\theta}}_{1:T}$. The initial hidden state is chosen to be $\mathbf{h}_0 = (1 - \tilde{I}_0, \tilde{I}_0, \mathbf{0})$, where $\mathbf{0}$ is a vector of 30 zeros. We also take $\mathbf{o}_0 = (\log(1 - \tilde{I}_0), \log(\tilde{I}_0), -\infty)$ which indexes the logits of the multinomial distribution at time $t = 0$. Once again, we may write the structural equations $\tilde{f}_{\tilde{\mathbf{y}}_t}$ for the $\tilde{\mathbf{y}}_t$ in terms of \tilde{I}_0 , $\tilde{\boldsymbol{\theta}}_{1:t}$, and the exogenous random variables $\tilde{\mathbf{u}}_t$ required to reparameterise the sampling procedure from the multinomial distribution.

Since we use exactly the same networks in this surrogate family as in the LODE-RNN family, the total number of trainable parameters from ψ and ϕ combined is also 13,798.

E.4 The likelihood function for each of these surrogate families

Having intervened on the \tilde{I}_0 and $\tilde{\boldsymbol{\theta}}_t$ with known values, the class probabilities for each multinomial distribution is completely determined given the deterministic dynamics within the structural equations mapping to the $\tilde{\mathbf{y}}_t$.

E.5 Formalising the τ map

Taking $\text{dom}[I_0] = \mathcal{J}_{\mathcal{M}} = [0, 1]$, $\text{dom}[\mathbf{X}_{0:T}] = \mathcal{X}^{T+1}$ with $\mathcal{X} = \{0, 1, 2\}^N$, and $\text{dom}[\boldsymbol{\Theta}_{1:T}] = \mathcal{P}_{\mathcal{M}}^T$ with $\mathcal{P} = [0, 1]^3$, we define

$$\tau : \mathcal{J}_{\mathcal{M}} \times \mathcal{X}^{T+1} \times \mathcal{P}_{\mathcal{M}}^T \rightarrow \mathcal{J}_{\mathcal{M}'} \times \mathcal{Y}^{T+1} \times \mathcal{P}_{\mathcal{M}'}^T$$

which operates componentwise as

$$\tau(I_0, \mathbf{x}_{0:T}, \boldsymbol{\theta}_{0:T}) = (\tau_i(I_0), \tau_x(\mathbf{x}_{0:T}), \tau_\theta(\boldsymbol{\theta}_{0:T})) \quad (29)$$

where

$$\tau_i = \text{id}, \quad (30)$$

$$\tau_x : \mathbf{x}_{0:T} \mapsto \left(\sum_{n=1}^N \mathbb{I}_{\mathbf{x}_{nt}=0}, \sum_{n=1}^N \mathbb{I}_{\mathbf{x}_{nt}=1}, \sum_{n=1}^N \mathbb{I}_{\mathbf{x}_{nt}=2} \right)_{0:T},$$

$$\tau_\theta = \text{id}. \quad (31)$$

In the above, id is the identity map, and τ_x acts by counting the total number of susceptible, infected, and recovered individuals in the ABM at each time step.

E.6 Further experimental details on the training procedure

All models were trained on a MacBook Pro using an Apple M2 Chip, operating on macOS Ventura 13.2.1. Software dependencies are specified in the GitHub repository containing the code for this paper, which will be made public upon acceptance.

We assume periodic boundary conditions in both spatial dimensions for the ABM presented in Example 1, which is used in all of our experiments.

For the LODE and LODE-RNN surrogate families, we forward simulate the SIRS ODE with an Euler scheme with step size $\Delta t = 1$.

For all surrogates, the neural networks comprising the ω^ϕ map and structural equations parameterised by ψ were trained with a learning rate of 10^{-2} for a maximum number of 1000 epochs, batch size $B = 50$, and with the Adam optimiser (Kingma and Ba, 2014). A total number of $R = 1000$ training samples was generated from the ABM for each of the observational and interventional training sets; these were each split 5 times into different training and validation sets of sizes 800 and 200, respectively, with a new surrogate model trained from scratch on each of these splits. We apply an early stopping criterion in which training is ceased if the validation error does not decrease for 20 consecutive epochs.



Figure 8: A schematic representation of the LRNN surrogate family for a single time step. First, the parameters θ_{t+1} are passed to a recurrent neural network (denoted by RNN in the diagram) that updates its hidden state. The updated hidden state is passed to a feedforward neural network (denoted by FF in the diagram), which computes the logits \mathbf{o}_{t+1} for a multinomial distribution from which $\tilde{\mathbf{y}}_{t+1}$ is sampled.